Submitted to: *Main Group Chemistry*

The Effect of Concentration and Post-Deposition Annealing on Silica Coated Germanium Quantum Dot Thin Films Grown by Vertical Deposition

Brittany L. Oliva-Chatelain,[a] and Andrew R. Barron,*[,a,b,c]

[a] *Department of Chemistry, Rice University, Houston, Texas 77005, USA*

[b] *Department of Materials Science and Nanoengineering, Rice University, Houston, Texas 77005, USA*

[c] *Energy Safety Research Institute (ESRI), College of Engineering, Swansea University, Bay Campus, Swansea, SA1 8EN, Wales, UK*

* Corresponding author. Tel.: +1-713-348-5610; E-mail: arb@rice.edu.

Abstract

Thin films have been grown using silica coated germanium quantum dot ($Ge@SiO_2$) nanoparticles (NP) as well as their phosphorus-doped analogues ($P\text{-}Ge@SiO_2$). The Ge quantum dots (QDs) were coated through the seeding of Stöber particles. The film thickness and uniformity were investigated using aqueous solutions of at a range of dilutions from the as prepared solutions. The films have been characterized by SEM, XRD, and I/V measurements of test solar cells using doped n-type Si substrates. While the films were relatively compact they are actually made of large plaques of particles rather than a continuous layer, and the film thickness showed little significant variation with concentration for the $Ge@SiO_2$ films; although a more usual trend was observed for the $P\text{-}Ge@SiO_2$ films. Films grown using a solution $^1/_4$ of the maximum concentration provided the highest solar cell efficiency. Thermal annealing the films prior to deposition of the front and back contacts enabled a doubling in the cell efficiency, but did not show any marked increase in the density or crystallinity of the films.

Keywords: silica; germanium; quantum dot; thin film; solar cell

1. Introduction

Colloidal crystals are three-dimensional assemblies of mono-dispersed spheres such as silica or polystyrene [1,2]. These assemblies have become an interest for applications in anti-reflective coatings, optical filters, and solar cells [3,4]. There are many methods to produce colloidal crystals, such as: gravity sedimentation, electrophoretic deposition, spin coating, centrifugation, capillary deposition, and vertical deposition [5-13]. One potential low cost and saleable approach has been recently studied for a wide range of films by spray deposition [14-16]. Gravity sedimentation takes weeks even on a small scale, so using that method for mass production would be time consuming and costly [5,11]. For the best control at the laboratory scale, the vertical deposition method appears to have the most success because it is the most reproducible and reliable method of the above mentioned; this method also does not require special equipment or environment to produce the array [9-13].

We have recently reported that germanium quantum dots (QDs) may be coated with silica via either a liquid phase deposition (LPD) process [17] or through the seeding of Stöber particles [18,19]. The formation of thin films on suitably doped silicon wafers enabled a hybrid solar cell device to be tested [19]. While device performance is dependent on a myriad of parameters, including the inter QD···QD distance, the doping of the QDs, and the conductivity of the silica matrix, we are interested in determining the effects of film formation and post deposition annealing on the device performance. We have therefore investigated the vertical deposition of silica coated Ge QD ($Ge@SiO_2$) nanoparticles (NPs). Using these particles will allow for a similar approach as that reported in literature since the particles are externally silica.

2. Experimental

2.1. Materials and methods

All materials were obtained commercially and were not further purified. Silica coated Ge QDs ($Ge@SiO_2$) were prepared by previously reported methods [18,19]. Quartz slides (75 x 25 x 1 mm^3) were obtained from Chem Glass. Indium tin oxide (ITO) coated glass slides (75 x 25 x 1

mm^3, 8-12 Ω/sq surface resistivity) came from Sigma Aldrich. The n-type silicon wafers were provided by Natcore Technology, Inc. (NXTV) with additional heavy phosphorus doping on the back to create a very conductive surface ready for the Au metal as a contact [19]. The wafers were passivated with silica to ensure the dopants remained in the wafers before use. The wafers were cut into 2 x 2 cm^2 pieces for experimental use. The oxide layer needed to be removed from each piece of wafer before thin films could be deposited, and the p-type wafers needed the excess aluminum paste to be removed as well to stop the aluminum from contaminating the particles during deposition. The wafers were cleaned in buffered oxide etchant for 3 minutes to remove the native oxide layer and the excess aluminum paste. The pieces were then cleaned with DI H_2O and plasma cleaned for 10 seconds to put a very thin oxide layer of about 10 nm back on the surface of the wafer. Without the thin oxide layer, the surface is too hydrophobic to allow the silica coated particles to come near the surface to create the thin film.

Characterization of the arrays was performed with a FEI Quanta 400 ESEM FEG scanning emission microscope equipped with an EDAX energy dispersive spectroscope. X-ray diffraction was performed on a Rigaku D/Max Ultima II configured with a vertical theta/theta goniometer, Cu-K_α radiation, graphite monochromator, and scintillation counter. Plasma cleaning was performed with a Plasma Cleaner 1020 equipped with Ar:O_2 (95:5) gas solution.

The efficiency of the QD/Si cells were calculated from the I-V curves detected via Keithley 2420 and 2425 High Current SourceMeter with an Oriel Model 81190 Solar simulator equipped with a Xenon lamp, including light intensity feedback control [19]. The intensity of incident light was 100 mW/cm^2. The solar cells were kept at a fixed distance of 6 inches from the light source for optimal conditions. The cells were attached to two leads, one connected to the back contact and the other connected to the busbar of the front contact [20]. This setup allowed for the measurement of the current produced by the cell with change in voltage.

2.3. Vertical deposition

To control the array best, a 2 x 2 cm^2 silicon wafer was placed vertically in a centrifuge tube with the coated QD solution (12 mL) having the wafer completely submerged. The solvent of the coated QD solution was DI H_2O to obtain the most control over the film. The solution with the wafer was then set to dry in a fume hood at the solvent's evaporation pace at room temperature. Not increasing the speed of evaporation with heat or vacuum allowed the particles to align themselves at the very top of the meniscus while the solvent dried slowly (Fig. 1) [10-13]. The solution with the wafer was sonicated briefly every couple of hours to ensure that the particles were evenly dispersed in the sample and not settling over time. In the case of Si wafer substrates, once the wafers are coated with the particles, a back contact of gold is added by sputtering. The front contact (gold or silver) is sputtered using a mask to create fingers across the surface without completely covering it with metal [20]. Both contacts are 100 nm thick, and the metal used depends on the identity of the dopant of the wafer and the presence of a QD containing layer [19].

[Insert Fig. 1 here]

To determine if the amount of material in the solution controlled the thickness of the thin film, several samples were made with varying concentrations of nanoparticles (NPs). Ge@SiO_2 NPss varied from 0.094-1.5 M, and P-Ge@SiO_2 NPs varied from 0.034-0.63 M. These concentrations were diluted with DI H_2O to keep everything consistent for comparison, and they were treated identically to the regular vertical deposition samples.

Annealing studies were performed on these samples. A set of four wafers was prepared with the same concentration of SiO_2@Ge NPs (0.375 M) to create four very similar thin films of the same material at the same concentration. These wafers were then each annealed at a different temperature for comparison. One was not annealed at all as a control sample. The second wafer was annealed at 200 °C under an inert atmosphere of argon in a sealed system in a tube furnace for 1 hr. The third wafer was treated similarly at 400 °C, and the fourth wafer was treated

similarly at 600 °C. These wafers were allowed to rest for 24 hr. after annealing to become reacclimated with the natural humidity of the atmosphere [21-24].

3. Results and discussion

3.1. Vertical deposition

We have previously deposited films of nanoparticles of silica coated Si QDs ($Si@SiO_2$ NPs) with an average particle size of 150 nm [17] by suspending in DI water with the substrate standing vertically, and the solution was evaporated on its own time at room temperature. Although the films appeared to be a glassy film, a closer view of the film showed that there were still gaps between the particles indicating that this was not a true array, and there was room for improvement [17]. The average particle center to particle center distance was 170 ±30 nm, consistent with a porous film. Other solvents were previously tested with this method [27], but none were found to be better than pure water. Furthermore, significantly smaller $Ge@SiO_2$ NPs have been produced and are required for solar cell applications [18,19]. Thus, it is expected that the packing of the particles and overall topology of the thin film may alter.

Fig. 2a shows the SEM image of a $Ge@SiO_2$ film grown from 1.5 M solution in DI H_2O. As may be seen by comparison with the results of an analogous growth of larger $Ge@SiO_2$ NPs (Fig. 2b), the film is more densely packed. However, the film is actually made of large plaques of particles rather than a continuous layer (Fig. 3). Such a cracked morphology is typically due to stresses upon solvent evaporation; however, it is interesting that this was not observed for the larger $Si@SiO_2$ particles. Presumably, lower particle···particle forces in the latter film mean that a lower density structure is formed (Fig. 2b). Obviously the plaque like structure is not appropriate for a device since metallization causes a short through the film, see below, Furthermore, not only are the plaques separated from each other in the plane of the substrate, but in some cases, the plaques are even separated and peeled up from the silicon wafer surface (Fig. 3). This separation also causes an issue with achieving higher efficiencies because whatever current the thin film generates cannot be transferred to the wafer to complete the circuit. Due to

these issues, concentration and annealing studies were done to determine if these problems could be combatted with slight modifications.

[Insert Fig. 2 here]

[Insert Fig. 3 here]

In order to determine if the concentration of the particle solution affected the uniformity as series of the films were grown with both $Ge@SiO_2$ and P-doped Ge QD derivatives (P-$Ge@SiO_2$). The concentrations of the as prepared (see Experimental) $Ge@SiO_2$ (1.5 mol/dm^3) and P-$Ge@SiO_2$ (0.63 mol/dm^3) NP solutions were determined from weight measurements after drying. This difference in NP concentration is most likely due to the change in QD surface with the presence of phosphorus [19]. A series of standard dilutions ($^1/_2$, $^1/_4$, $^1/_8$, and $^1/_{16}$ of the original solutions) were prepared to determine if there is a correlation between concentration and film thickness and/or continuity.

Fig. 4 shows top and cross sectional views of films grown from different concentration solutions of $Ge@SiO_2$ NPs. Regardless of the concentration of the particles, the packing between the particles remains constant and relatively close, resulting in a dense film. However, as the concentration decreased, the uniformity of the film decreased. More importantly, in most of the films, regardless of concentration, plaques of particles were still formed with the exception of the lowest concentration of $Ge@SiO_2$ NPs (0.094 mol/dm^3). The non-uniform nature of the films may be a consequence of the slow rate of film growth (days). In order for the NPs not to precipitate out of solution through aggregation, the reaction must be sonicated. This sonication may result in the damage of the grown film and the loss of fragments to the solution.

[Insert Fig. 4 here]

The graph in Fig. 5 shows that little to no correlation between concentration and film thickness of Ge@SiO_2 particles, except for the lowest concentration. It is worth noting that it is only at the lowest and highest concentrations that uniform films (small standard deviation in thickness) are formed. We have previously observed that too rapid an evaporation rate can cause the surface of the film show wave-like features [17]. This is not the case here, instead there is an inhomogeneous film growth; however, the NP···NP interaction compared to the NP···solvent interaction has been discussed as a controlling factor in film uniformity [8]. Although there is an obviously smaller film thickness with the lowest concentration of particles, the film also covered much less of the wafer. Higher concentrations could not be studied since even at 1.5 mol/dm^3 the particles have a hard time staying in solution.

[Insert Fig. 5 here]

The same experiments were performed with the phosphorus-doped quantum dots coated with silica (P-Ge@SiO_2). The base solution of these particles is lower than that of the undoped analogs; however, a similar trend is observed for the films grown. SEM images of the top and cross sectional views for films grown from each concentration are shown in Fig. 6. It is clear that these are very similar to the undoped films with plaques of close packed particles that are not touching each other or sometimes not touching the wafer. The variation of film thickness with the concentration of P-Ge@SiO_2 NP solution is shown in Fig. 7. Here there is the more expected trend, but again the variation in film thickness within a sample is wide.

[Insert Fig. 6 here]

[Insert Fig. 7 here]

We have previously demonstrated [19] that both the $Ge@SiO_2$ and P- $Ge@SiO_2$ NP thin films deposited on n-type Si wafers (see Experimental) allow for the fabrication of low efficiency (as a consequence of film uniformity) solar cells of the type defined as $Ag|Ge@SiO_2|n\text{-}Si|Au$ shown in Fig. 8. $Ge@SiO_2$ and P-$Ge@SiO_2$ NP thin film layers were deposited on n-type wafers with silver front and gold back contacts. The I/V curves were measured for these cells (see Fig. 9). As may be seen from Table 1, the as synthesized concentrations used previously [19] were not determined to be the optimal concentration for either $Ge@SiO_2$ or the P-doped homologs. Despite each type of NP having a different as-synthesized concentration ($Ge@SiO_2$ = 1.5 mol/dm^3 and P-$Ge@SiO_2$ = 0.63 mol/dm^3) the best devices were fabricated using films with a quarter of the natural concentration. The difference in the as-synthesized concentrations is not due to the pH of the QD solutions; as both reagent solutions are at pH 3.9. It can be observed that the incorporation of PCl_3 into the reaction mixture used for synthesizing the QDs (a toluene solution of $GeCl_4$ and $LiAlH_4$ in the presence of tetraoctylammonium bromide) slows the initiation of the reaction down (hours versus minutes) and the resulting material is a lot less concentrated. Although these two sets of particles are at two very different concentrations, the relative natural concentration ratio of their highest efficiencies is the same as seen in Fig. 10.

[Insert Fig. 8 here]

[Insert Fig. 9 here]

[Insert Fig. 10 here]

The plot in Fig. 10 raises two interesting points. First, for both QDs the best devices are produced using films grown from $^1/_4$ of highest concentration; even though the absolute values are different. We propose this is related to solutions at some value below the saturation point,

and therefore the deposition rate is more controllable. At lower concentrations presumably the quality of the films is too variable for a suitable cell. This is most likely the reason for the second observation, that the values of devices are produced using films grown from $^{1}/_{8}$ appear worse than the more dilute solutions. Given the potential of short-circuiting the cells with incomplete coverage, this is most probably an anomaly.

3.2. Annealing studies.

In an effort to densify the films, we have investigated thermal anneal in a stepwise manner. Based upon prior results with silica particles [21,22] we first annealed the samples to 200 °C, which has been reported to remove the residual water between particles without giving them enough energy to move closer [21,22]. Heating to 400 °C has been reported to aid in packing the thin film better [21]. Finally it has been reported that heating to 600 °C results in the initiation of melting of the particles resulting in a change of shape. The latter would be considered sintering rather than annealing but could still be considered useful since the quantum dots are randomly placed in the silica particles [18] and removing any space between the particles could create a quantum dot impregnated glass [21-25].

SEM images of the top and cross-sectional images of Ge@SiO_2 films grown from 0.38 mol/dm^3 solution after annealing at various temperatures is shown in Fig. 11. There was not much of a difference between any of the samples to be able to definitively say that the temperature has a real effect on the films as seen in the graph of Fig. 12. However, it is worthy to note that in the 600 °C film there were a few areas where particles could not be discerned, and it appeared as though there were solid pieces of material instead of aggregates of NPs, as seen in Fig. 11d.

[Insert Fig. 11 here]

[Insert Fig. 12 here]

XRD analysis of the films also showed that there is little change in the their crystallinity upon annealing. The XRD data shows silicon (002) at 33.2 2θ, while the silver from the front contacts and aluminum from the sample holder showed a broader peak due to the closeness of the peaks with Ag (111) at 38.2 2θ and Al (111) at 38.5 2θ. Regardless, these annealed films were studied for efficiency improvements, and the results are shown in Table 2. Two sets of samples were run. First, samples were annealed after deposition, but before the front and back contacts were deposited, i.e., Ge@SiO_2|n-Si. Second, thermal annealing was undertaken after the front and back contact were added, i.e., Ag|Ge@SiO_2|n-Si|Au. The data reveals that irrespective of at what stage the annealing was performed, heating to 400 °C gave the most enhancement in the cell efficiency. However, the increase in efficiency for the cell with contacts is only 28% over the as deposited film, while the cell without contacts efficiency increases 100% indicating a stronger argument for annealing the solar cells before placing the contacts on them.

[Insert Table 2 here]

4. Conclusions

Despite the vertical deposition method being faster than the evaporation process previously employed, none of the films created were ideal regardless of thickness or annealing. The best results with regard the test cell performance where at a concentration a quarter of the saturated concentrations of the NPs. However, under that level of dilution, the particles were too dispersed to make a reliable connection, and the efficiencies decreased beyond that point. Annealing also proved useful at 400 °C especially if the annealing was performed before the metal contact was applied.

It is interesting to note that the Ge@SiO_2 NPs formed from the Stöber synthesis [18] all produce lower quality porous films than those that use the liquid phase deposition (LPD) process [17]. Given that the LPD process involves the generation of HF as a side product and this results

in a continual growth/etch process [28], we propose that the LPD growth of dense thin films offers benefits over the Stöber synthesis. It would be interesting to combine these solutions with a spray process [14-16]. Finally, we note that aerosol assisted chemical vapor deposition (AACVD) may be the best option for a uniform array. AACVD would also allow for a completely glassy layer to be produced [29-31]. One particular report creates phosphorus-doped germanium using this method, so it is possible to use this method for solar cells [31]. Additionally, this method can be completely customized with QD concentration, precise glass layer thickness, and atmosphere control to ensure that the QDs will not oxidize at the higher temperatures required for this method.

Acknowledgments

Financial support was provided by the Robert A. Welch Foundation (C-0002) and the Welsh Government Sêr Cymru Programme. The authors would also like to thank Desmond Schipper and Kenton Whitmire for their assistance with the XRD data.

References

[1] A. Wang, S.-L. Chen, and P. Dong, Rapid fabrication of a large-area 3D silica colloidal crystal thin film by a room temperature floating self-assembly method, *Mater. Lett.* **63** (2009), 1586-1589.

[2] A. Stein, B. E. Wilson, and S. G. Rudisill, Design and functionality of colloidal-crystal-templated materials—chemical applications of inverse opals, *Chem. Soc. Rev.* **42** (2013), 2763-2803.

[3] U. Jonas and C. Krüger, The effect of polar, nonpolar, and electrostatic interactions and wetting behavior on the particle assembly at patterned surfaces, *J. Supramol. Chem.* **2** (2002), 255-270.

[4] H. Cong, B. Yu, J. Tang, Z. Li, and X. Liu, Current status and future developments in preparation and application of colloidal crystals, *Chem. Soc. Rev.* **42** (2013), 7774-7800.

[5] D. Mei, H. Liu, B. Cheng, Z. Li, and D. Zhang, Visible and near-infrared silica colloidal crystals and photonic gaps, *Phys. Rev. B* **58** (1998), 35-38.

[6] R. Mayoral, J. Requena, J. Moya, C. Lopez, A. Cintas, H. Miguez, F. Meseguer, L. Vazquez, M. Holgado, and A. Blanco, 3D Long-range ordering in ein SiO_2 submicrometer-sphere sintered superstructure, *Adv. Mater.* **9** (1997), 257-260.

[7] W. Wen, N. Wang, H. Ma, Z. Lin, W. Y. Tam, C. T. Chan, and P. Sheng, Field induced structural transition in mesocrystallites, *Phys. Rev. Lett.* **82** (1999), 4248-4251.

[8] M. Cortalezzi, V. Colvin, and M. Wiesner, Controlling submicron-particle template morphology: effect of solvent chemistry, *J. Colloid Interf. Sci.* **283** (2005), 366-372.

[9] Y. Min, M. Akbulut, K. Kristiansen, Y. Golan, and J. Israelachvil, The role of interparticle and external forces in nanoparticle assembly, *Nat. Mater.* **7** (2008), 527-538.

[10] F. Piret, and B.-L. Su, Effects of pH and ionic strength on the self-assembly of silica colloids to opaline photonic structures, *Chem. Phys. Lett.* **457** (2008), 376-380.

[11] T. H. Kim, H. J. Kim, T. S. Lee, and W. S. Lyoo, Diffraction color developed by self-assembly of silica particle arrays, *Mol. Cryst. Liq. Cryst.* **464** (2007), 153-159.

[12] J. Yang, T. J. Barbarich, and A. R. Barron, SiO_2 template-derived polyurethane and alumina nanoparticle-polyurethane lithium ion separator membranes, *Main Group Chem.* **12** (2013), 45-56.

[13] H.-L. Li and F. Marlow, Solvent effects in colloidal crystal deposition, *Chem. Mater.* **18** (2006), 1803-1810.

[14] F. Bouaichi, H. Saidi, A. Attaf, M. Othmane, N. Lehraki, M. Nouadji, M. Poulain, and S. Benramache, The synthesis and characterization of sprayed ZnO thin films: As a function of solution molarity, *Main Group Chem.* **15** (2015), 57-66.

[15] Y. Aoun, B. Benhaoua, B. Gasmi, and S. Benramache, Study the structural, optical and electrical properties of sprayed zinc oxide (ZnO) thin films before and after annealing temperature, *Main Group Chem.* **14** (2015), 27-33.

[16] O. Belahssen, S. Benramache, and B. Benhaoua, Effect of Urbach energy with precursor molarity on the crystallite size in undoped ZnO thin film, *Main Group Chem.* **13** (2014), 343-352.

[17] B. L. Oliva and A. R. Barron, Thin films of silica imbedded silicon and germanium quantum dots by solution processing, *Mat. Sci. Semicon.* **15** (2012), 713-721.

[18] H. Rutledge, B. L. Oliva-Chatelain, S. J. Maguire-Boyle, D. L. Flood, and A. R. Barron, Imbedding germanium quantum dots in silica by means of a modified Stöber method, *Mat. Sci. Semicon. Proc.* **17** (2013), 7-12.

[19] B. L. Oliva-Chatelain and A. R. Barron, Experiments towards size and dopant control of germanium quantum dots for solar applications, *AIMS Mater. Sci.* **3** (2016), in press.

[20] Y.-T. Lu and A. R. Barron, In-situ fabrication of a self-aligned selective emitter silicon solar cell using the gold top contacts to facilitate the synthesis of a nanostructured black silicon anti-reflective layer instead of an external metal nanoparticle catalyst, *ACS Appl. Mater. Interfaces*. **7** (2015), 11802–11814.

[21] F. Gallego-Gomez, A. Blanco, and C. Lopez, In situ optical study of water sorption in silica colloidal crystals, *J. Phys. Chem. C* **116** (2012), 18222-18229.

[22] A. K. Gathania, N. Dhiman, A. Sharma, B. P. Singh, Development and annealing of colloidal multilayer structures of silica microspheres, *Colloid Surface A* **378** (2011), 34-37.

[23] S. Inai, A. Harao, and H. Nishikawa, Correlation between the luminescence properties and the surface structures of submicron silica particles, *J. Non-Cryst. Solids* **353** (2007), 510-513.

[24] M. D. Sacks and T. Y. Tseng, Preparation of Sio_2 glass from model powder compacts: II, sintering, *J. Am. Ceram. Soc.* **67** (1984), 532-537.

[25] T. Yokoi, J. Wakabayashi, Y. Otsuka, W. Fan, M. Iwama, R. Watanabe, K. Aramaki, A. Shimojima, T. Tatsumi, and T. Okubo, Mechanism of formation of uniform-sized silica nanospheres catalyzed by basic amino acids, *Chem. Mater.* **21** (2009), 3719-3729.

[26] J. Wang, A. Sugawara-Narutaki, M. Fukao, T. Yokoi, A. Shimojima, and T. Okubo, Two-phase synthesis of monodisperse silica nanospheres with amines or ammonia catalyst and their controlled self-assembly, *Appl. Mater. Interfaces* **3** (2011), 1538-1544.

[27] B. L. Oliva, Regular arrays of QDs by solution processing, MSc Thesis, Rice University, 2011.

[28] E. A. Whitsitt and A. R. Barron, Effect of surfactant on particle morphology for liquid phase deposition of submicron silica, *J. Colloid Interface Sci*. **287** (2005), 318-325.

[29] N. Alam, M. S. Hill, G. Kociok-Kohn, M. Zeller, M. Mazhar, and K. C. Molloy, Pyridine adducts of nickel(II) xanthates as single-source precursors for the aerosol-assisted chemical vapor deposition of nickel sulfide, *Chem. Mater*. **20** (2008), 6157-6162.

[30] J. M. Clark, G. Kociok-Kohn, N. J. Harnett, M. S. Hill, R. Hill, K. C. Molloy, H. Saponia, D. Stanton, and A. Sudlow, Formation of PbS materials from lead xanthate precursors, *Dalton Trans*. **40** (2011), 6893-6900.

[31] L. Apostolico, M. F. Mahon, K. C. Molloy, R. Binions, C. S. Blackman, C. J. Carmalt, and I. P. Parkin, The reaction of $GeCl_4$ with primary and secondary phosphines, *Dalton Trans*. **3** (2004), 470-475.

Table 1

Concentration studies of untreated $Ge@SiO_2$ and P-$Ge@SiO_2$.

QD	Actual concentration (mol/dm^3)	Relative concentration	Efficiency (%)
$Ge@SiO_2$	1.5	1	0.0025
	0.75	1/2	0.0004
	0.38	1/4	0.013
	0.19	1/8	0.000
	0.09	1/16	0.011
P-$Ge@SiO_2$	1.26	2	0.0014
	0.63	1	0.0093
	0.32	1/2	0.018
	0.16	1/4	0.033
	0.08	1/8	0.0002
	0.04	1/16	0.0045

Table 2

Annealing studies with solar cells.

Sample	Annealing temperature (°C)	Efficiency (%)
Ge@SiO_2|n-Si[a]	untreated	0.0075
	200	0.0000
	400	0.0150
	600	0.0000
Ag|Ge@SiO_2|n-Si|Au	untreated	0.0025
	200	0.0016
	400	0.0032
	600	0.0010

[a] Silver front and gold back contacts were deposited after thermal treatment.

Legends for Figures

Fig. 1. Schematic of vertical deposition technique.

Fig. 2. SEM image of particles in a typical (a) $Ge@SiO_2$ QDs (d = 17 nm) deposited on a n-type Si wafer substrate from DI water suspension compared with (b) larger $Si@SiO_2$ QDs (d = 150 nm) deposited under similar conditions (used with permission from ref. 17. Copyright: Elsevier 2012).

Fig. 3. SEM images of (a) the surface and (b) the cross-section of a typical $Ge@SiO_2$ QD thin film grown on n-type Si wafer from DI water suspension.

Fig. 4. SEM surface and cross-sectional images of films formed from varying concentrations of $Ge@SiO_2$ NPs solutions in DI H_2O: 1.50 mol/dm^3 (a and f), 0.750 mol/dm^3 (b and g), 0.375 mol/dm^3 (c and h), 0.188 mol/dm^3 (d and i), and 0.094 mol/dm^3 (e and j).

Fig. 5. Film thickness versus concentration of $Ge@SiO_2$ NPs.

Fig. 6. SEM surface and cross-sectional images of films formed from concentrations of P-$Ge@SiO_2$ NPs. NPs solutions in DI H_2O: 0.630 mol/dm^3 (a and f), 0.315 mol/dm^3 (b and g), 0.158 mol/dm^3 (c and h), 0.079 mol/dm^3 (d and i), and 0.034 mol/dm^3 (e and j).

Fig. 7. Film thickness versus concentration of P-$Ge@SiO_2$ NPs.

Fig. 8. Schematic representations of the Au|$Ge@SiO_2$|n-Si|Ag test devices.

Fig. 9. Representative I/V curves measured for (a) Ag|Ge@SiO_2|n-Si|Au (solid line) and (b) Ag|P-Ge@SiO_2|n-Si|Au (dashed line).

Fig. 10. Cell efficiencies for (a) Ag|Ge@SiO_2|n-Si|Au (black) and (b) Ag|P-Ge@SiO_2|n-Si|Au (grey) at varying relative concentrations of the NP solutions used to grow the films.

Fig. 11. SEM surface and cross-sectional images of as deposited Ge@SiO_2 NP thin films (a and e) as compared to those annealed to 200 °C (b and f), 400 °C (c and g), and 600 °C (d and h) for 1 h at each temperature.

Fig. 12. Film thickness as a function of anneal temperature for Ge@SiO_2 NP thin films.

Fig. 1.

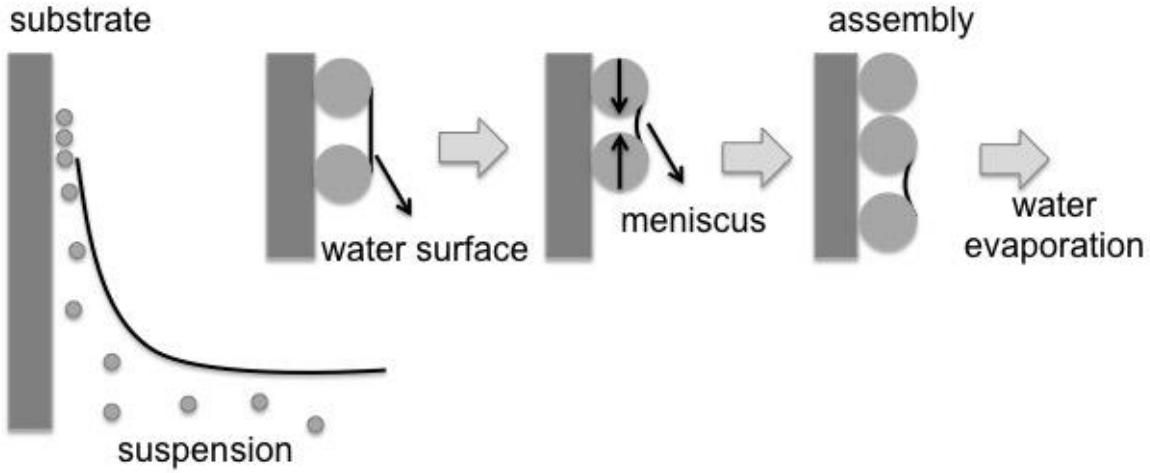
substrate
assembly
water surface
meniscus
water
evaporation
suspension

Fig. 2.

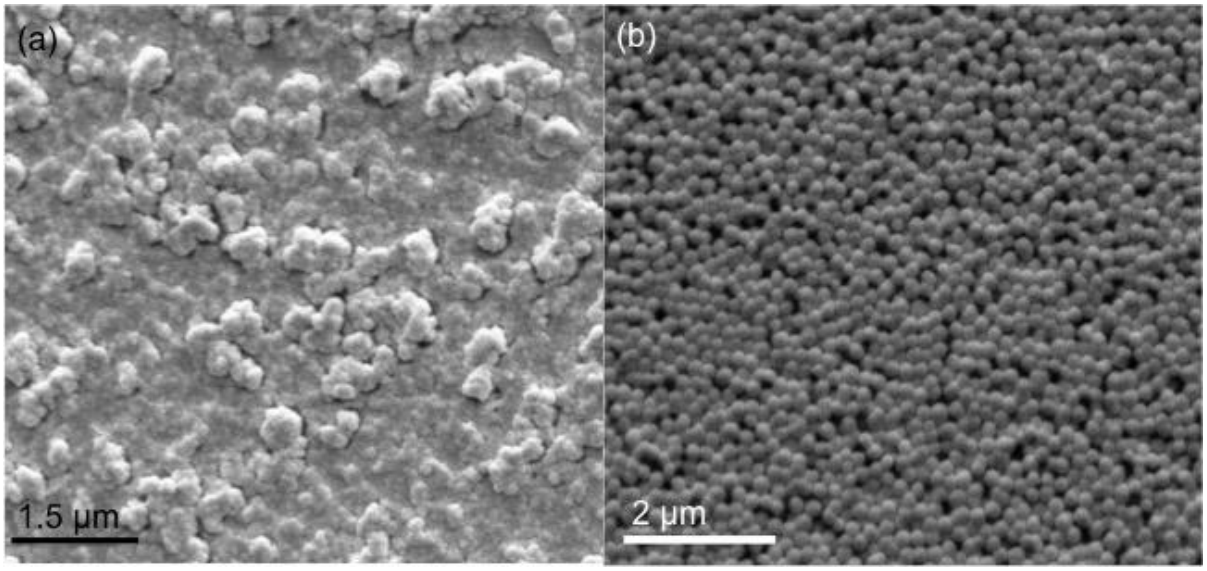

Fig. 3.

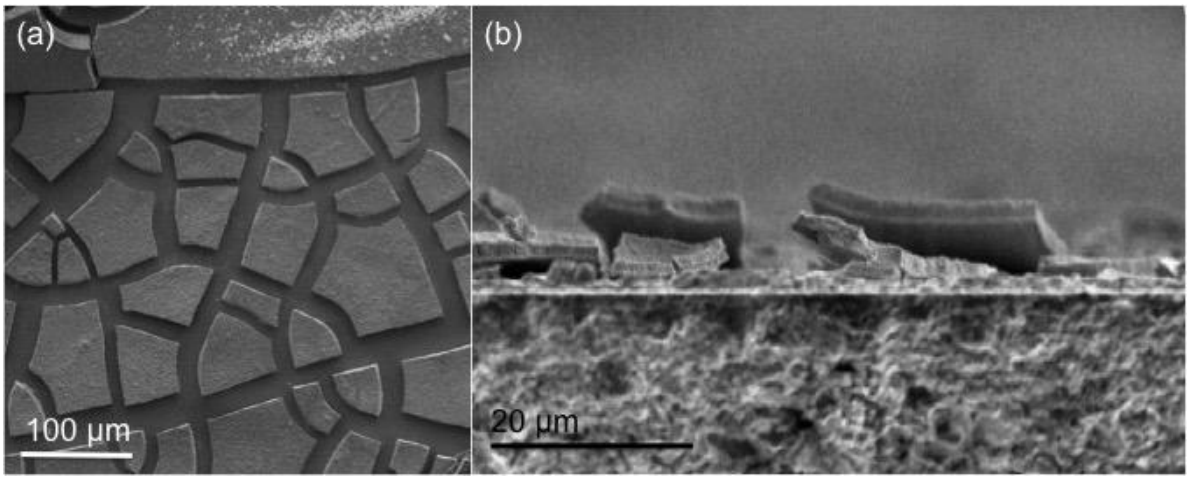

Fig. 4.

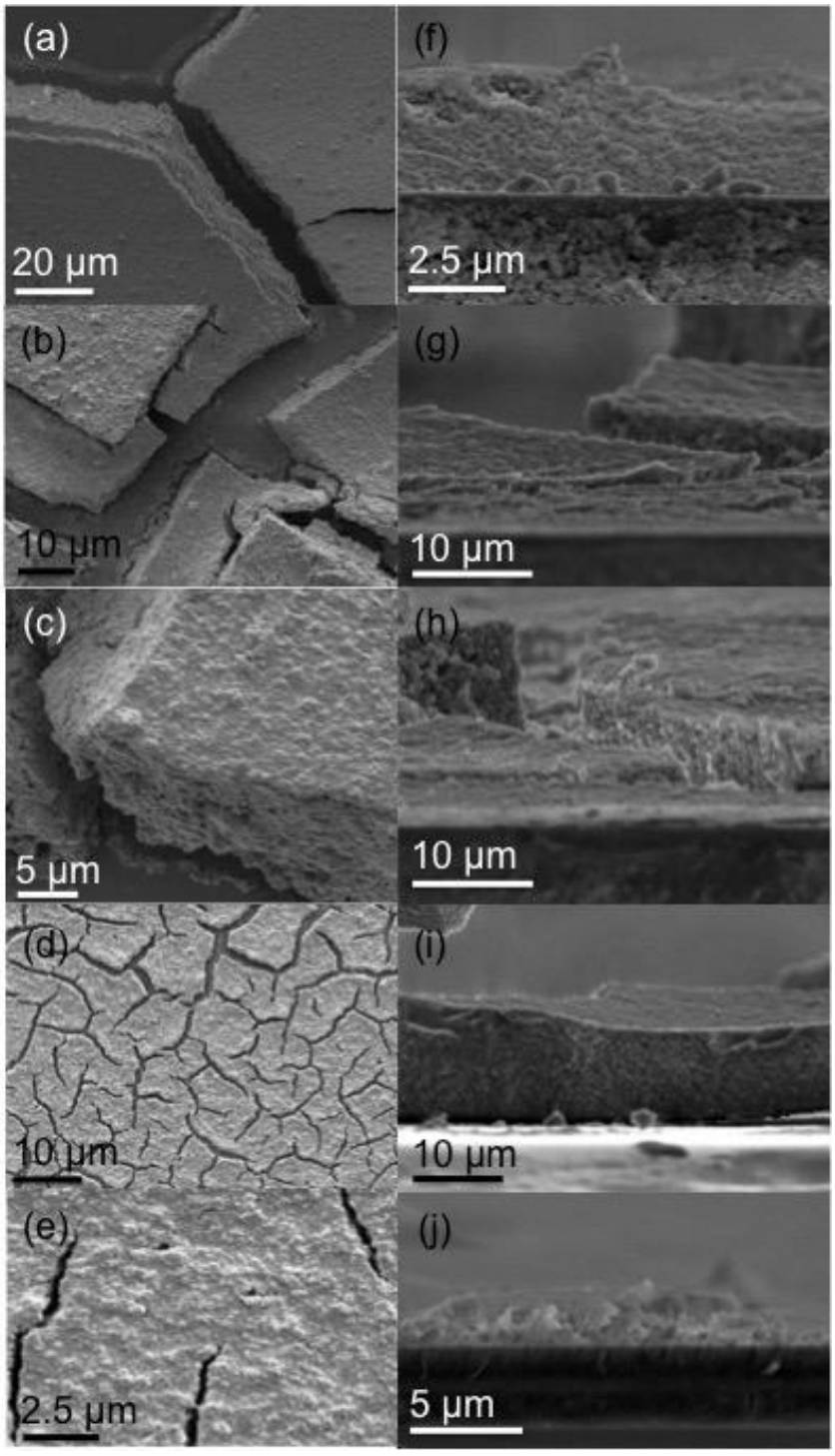

Fig. 5.

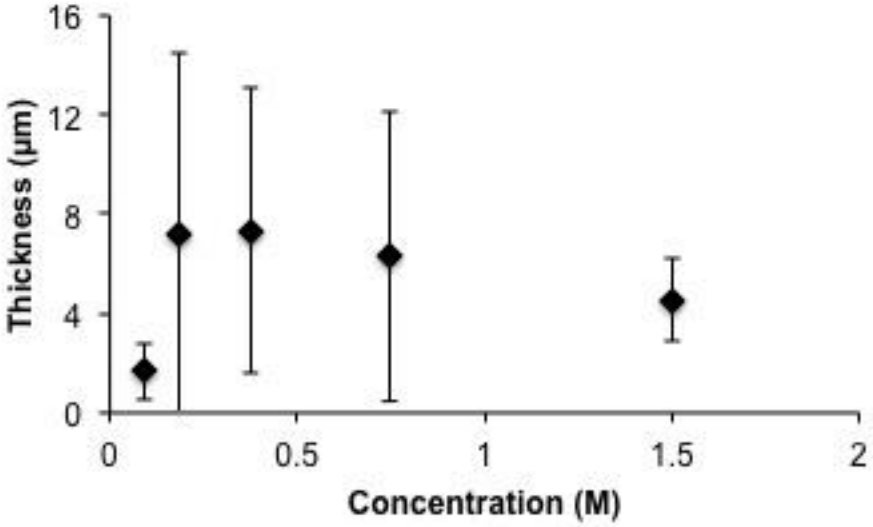

Fig. 6.

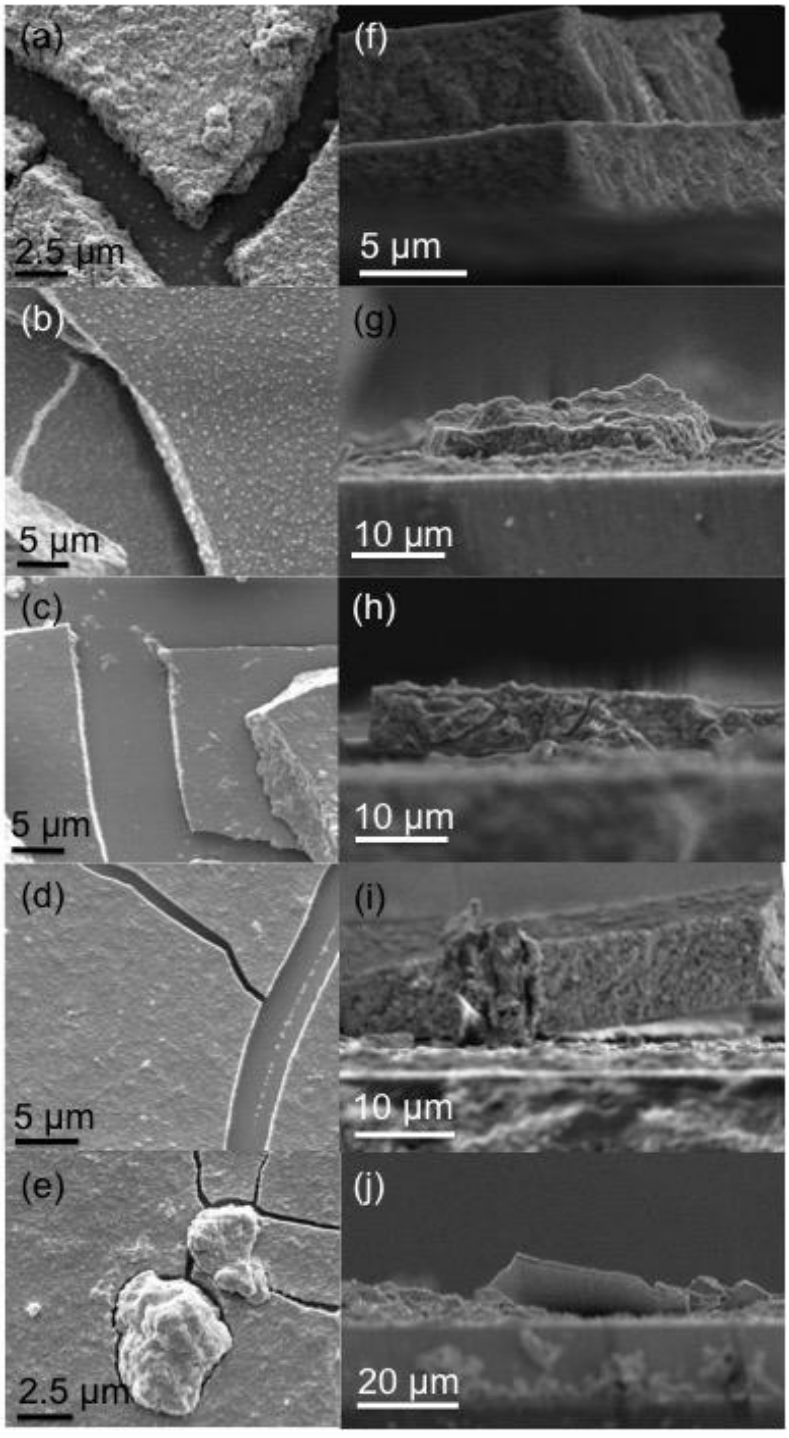

Fig. 7

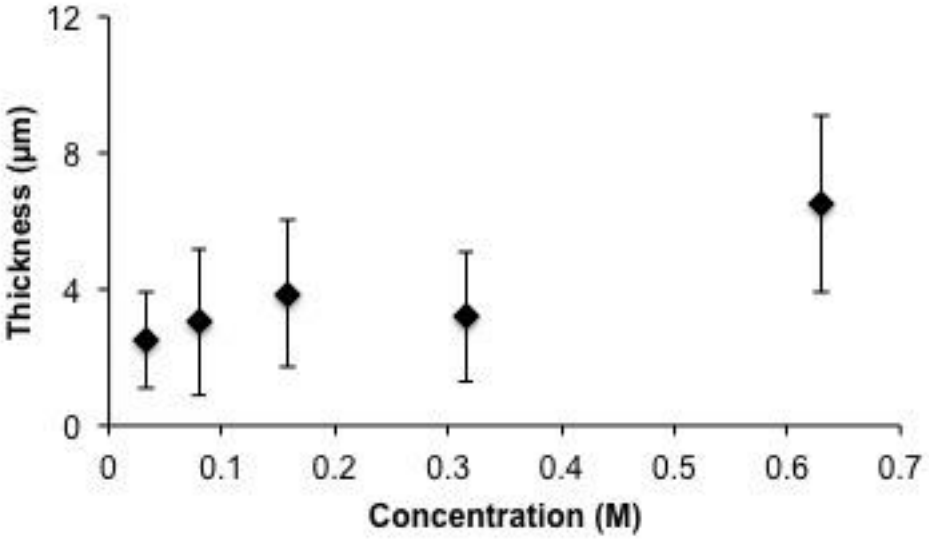

Fig. 8.

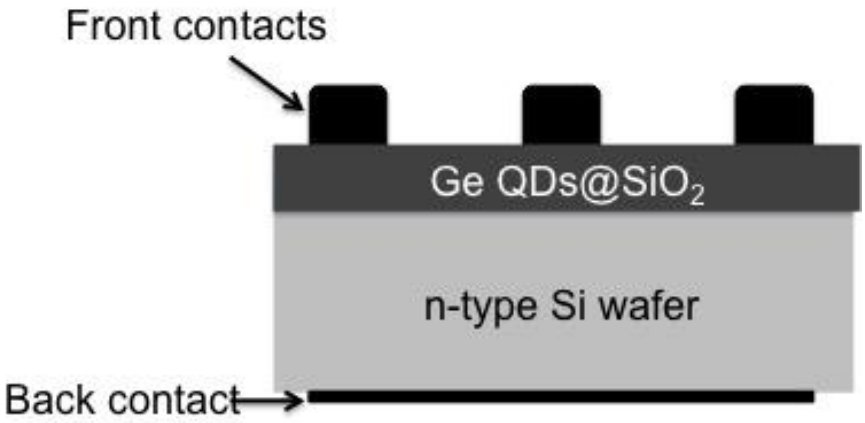

Fig. 9.

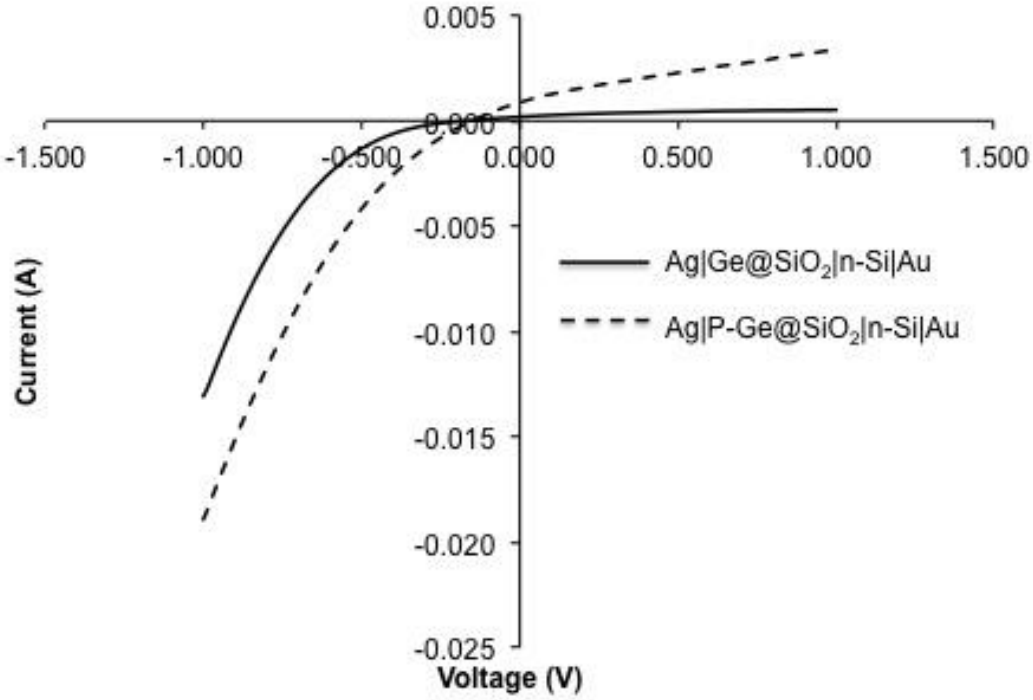
0.005
0.000
-0.005
-0.010
-0.015
-0.020
-0.025
-1.500
-1.000
-0.500
0.000
0.500
1.000
1.500
Current (A)
Voltage (V)
Ag|Ge@SiO2|n-Si|Au
Ag|P-Ge@SiO2|n-Si|Au

Fig. 10.

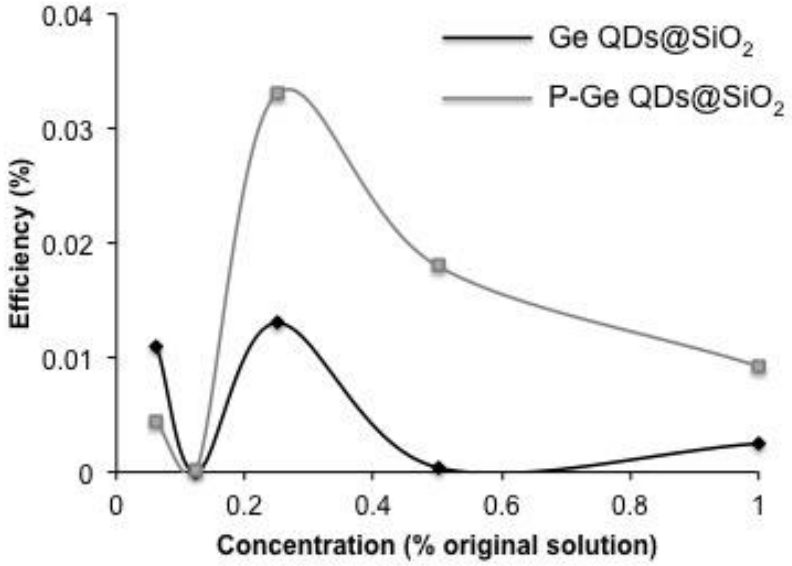
0.04
0.03
0.02
0.01
0
Efficiency (%)
0
0.2
0.4
0.6
0.8
1
Concentration (% original solution)
Ge QDs@SiO2
P-Ge QDs@SiO2

Fig. 11.

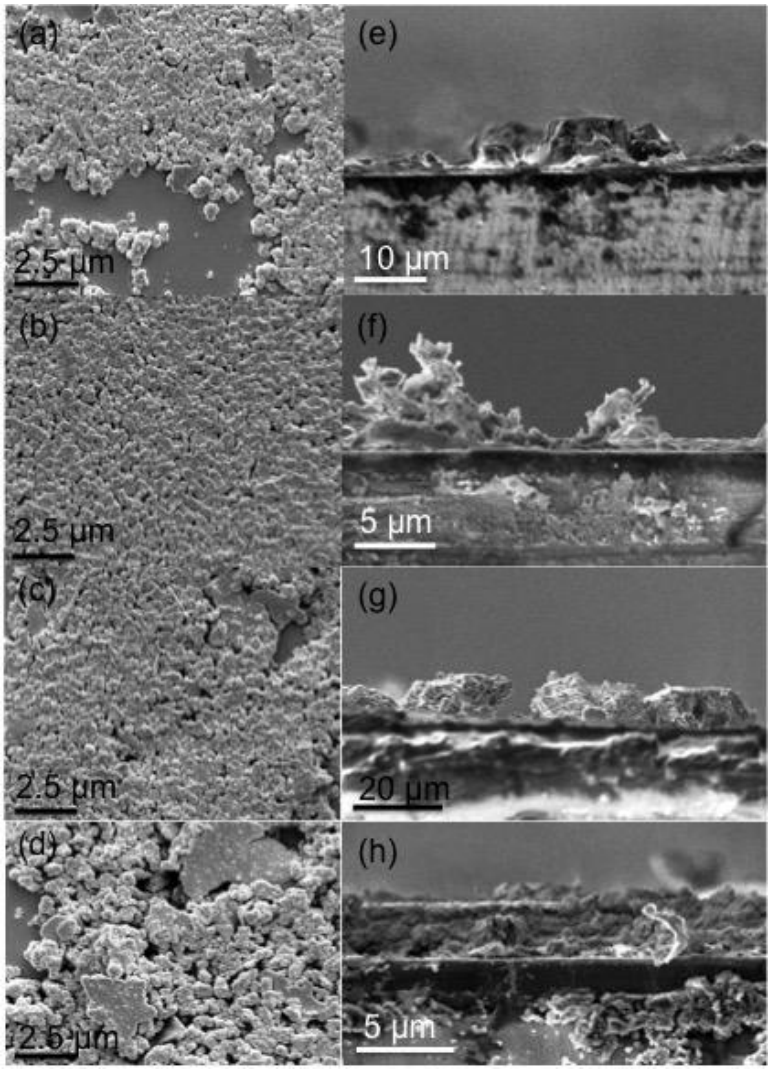

Fig. 12.

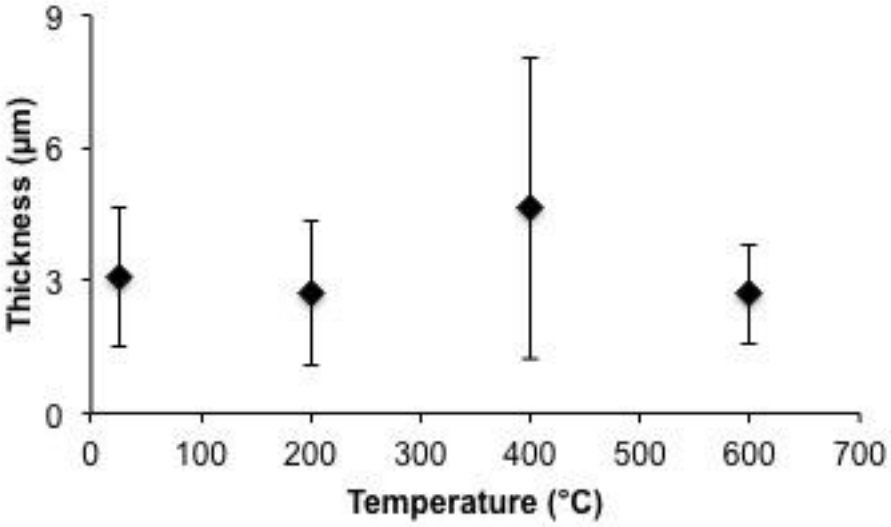

Artistic Pic: